



OPEN

# The stability and electronic properties of novel three-dimensional graphene-MoS<sub>2</sub> hybrid structure

Zhen-Kun Tang<sup>1,2</sup>, Yan-Ning Zhang<sup>1,3</sup>, Deng-Yu Zhang<sup>2</sup>, Woon-Ming Lau<sup>1,3</sup> & Li-Min Liu<sup>1</sup><sup>1</sup>Beijing Computational Science Research Center, Beijing 100084, China, <sup>2</sup>Departments of Physics and Electronics, Hengyang Normal University, Hengyang 421008, China, <sup>3</sup>Chengdu Green Energy and Green Manufacturing Technology R&D Center, Chengdu, Sichuan, 610207, China.

Three-dimensional (3D) hybrid layered materials receive a lot of attention because of their outstanding intrinsic properties and wide applications. In this work, the stability and electronic structure of three-dimensional graphene-MoS<sub>2</sub> (3DGM) hybrid structures are examined based on first-principle calculations. The results reveal that the 3DGMs can easily self-assembled by graphene nanosheet and zigzag MoS<sub>2</sub> nanoribbons, and they are thermodynamically stable at room temperature. Interestingly, the electronic structures of 3DGM are greatly related to the configuration of joint zone. The 3DGM with odd-layer thickness MoS<sub>2</sub> nanoribbon is semiconductor with a small band gap of 0.01–0.25 eV, while the one with even-layer thickness MoS<sub>2</sub> nanoribbon exhibits metallic feature. More importantly, the 3DGM with zigzag MoS<sub>2</sub> nanoribbon not only own the large surface area and effectively avoid the aggregation between the different nanoribbons, but also can remarkably enhance Li adsorption interaction, thus the 3DGM have the great potential as high performance lithium ion battery cathodes.

SUBJECT AREAS:  
SURFACES, INTERFACES  
AND THIN FILMS  
ELECTRONIC PROPERTIES AND  
MATERIALSReceived  
14 August 2014Accepted  
3 October 2014Published  
12 November 2014Correspondence and  
requests for materials  
should be addressed to  
L.-M.L. (limin.liu@csrc.  
ac.cn)

Over the last decade, graphene, the thinnest two-dimensional (2D) material, has aroused tremendous research interest because of its excellent mechanical, thermal, electronic and optical properties<sup>1–4</sup>. Many of outstanding properties of graphene are closely related to its atomic-layer thickness and large surface areas<sup>5–8</sup>. However, graphene tends to form irreversible agglomerates or even restack to form graphite through strong  $\pi$ - $\pi$  stacking and Van der Waals (vdW) interactions<sup>9</sup>. To fully utilize the high intrinsic surface area of graphene, novel three dimensional (3D) graphene networks have attracted extensive experimental attention, particularly in synthesis<sup>10–14</sup>. For example, Cao *et al.* first reported the preparation of 3D graphene networks by using Ni foam as a sacrificial template in a facile chemical vapor deposition (CVD) process with ethanol as the carbon source<sup>11</sup>. Their experimental results indicated that 3D graphene network can serve as a good platform to construct graphene/metal oxide composites for supercapacitor applications. Subsequently, Dong *et al.* demonstrated the use of 3D graphene foam as a novel free-standing and monolithic electrochemical electrode for electrochemical sensor<sup>12</sup>. Wang *et al.* developed a sugar-blowing approach to effectively synthesize a 3D graphene product, which further allows avoiding disintegration and performance decay in any scaled-up device fabrication process<sup>14</sup>. Overall, 3D graphene has large surface areas, high stability and good conductivity, which is promising as matrices for the further improvement of the electrochemical and electrocatalytic performance in metal oxides and metal sulfides.

Strikingly, high performance energy storage properties have already been observed in many hybrid 3D graphene-oxide systems when stacking with the oxides of MnO<sub>2</sub><sup>15</sup>, Co<sub>3</sub>O<sub>4</sub><sup>16</sup>, SnO<sub>2</sub><sup>17</sup> and so on. It is well known that MoS<sub>2</sub> monolayer is a typical 2D layered structure with a direct band gap of 1.8 eV<sup>18</sup>, which is suitable for industrial catalyst<sup>19–21</sup> and rechargeable Li-ion batteries<sup>22–25</sup>. Recent experiments<sup>26,27</sup> suggest that the 3D graphene-MoS<sub>2</sub> (3DGM) hybrid structures show good cycling and excellent high-current-density performances, which depicts a 10th-cycle capacity of 466 mAhg<sup>-1</sup> at a high current density of 4 Ag<sup>-1</sup>. The physical mechanism behind this experimental observation needs more theoretical investigations.

Many theoretical studies have been performed on 3D layered structures. Jiang *et al.* constructed 3D graphene structures by zigzag or armchair graphene nanoribbons as building blocks and sp<sup>3</sup> carbon chains as junction nodes<sup>28</sup>. In the meanwhile, 3D BN<sup>29</sup> and MoS<sub>2</sub><sup>30</sup> structures have also been predicted by density functional theory (DFT) calculations. However, to the best of our knowledge, no theoretic study as yet has been reported on the 3D graphene hybrid structures.



In this work, we proposed a novel 3DGM model that contains graphene nanosheets and MoS<sub>2</sub> nanoribbons as building blocks. The thermodynamics stability, electronic properties, and Li adsorption and diffusion are further calculated based on first principle calculations. The calculation results show that the 3DGM hybrid structures are thermodynamically stable at room temperature. The electronic properties of 3DGM are closely related to the geometric constructions of joint zone, showing an obvious odd-even change with the number of atomic layer in MoS<sub>2</sub> nanoribbon. Interestingly, the 3DGM hybrid structures are beneficial for providing a smooth transfer of foreign mass within the bubble channels and for retaining the intrinsic properties of the building blocks. The zigzag MoS<sub>2</sub> building blocks remain the enhanced lithium absorption and diffusion characteristics of zigzag MoS<sub>2</sub> nanoribbons. Because of its high stability, huge surface areas and excellent intrinsic properties, the 3DGM hybrid structures, which are promising candidates as the cathode material for high-performance lithium-ion batteries, might be also used for other clean energy applications, such as electrocatalytic hydrogen production.

## Results

**The geometrical construction and stability of the 3DGM.** The initial 3DGM supercell is constructed by combining one graphene monolayer and *n*-layer MoS<sub>2</sub> nanoribbon. Clearly, its structure varies with the width and edge of MoS<sub>2</sub> nanoribbon, which can be either zigzag or armchair. In the following, we will discuss the different 3DGM structures with different edges (zigzag and armchair) and different thickness. For simplicity, a 3DGM structure that contains *n* atom-layer thickness zigzag (armchair) MoS<sub>2</sub> nanoribbon is denoted as 3DGM-*n*Z (3DGM-*n*A) in the following. Seven representative models, 3DGM-2Z, 3DGM-3Z, 3DGM-4Z, 3DGM-5Z, 3DGM-3A, 3DGM-4A, and 3DGM-5A, are examined in this work. For example, the 3DGM-3Z presents the system contains 3 atom-layer zigzag MoS<sub>2</sub> and graphene. To avoid the interaction between the MoS<sub>2</sub> nanoribbons in adjacent supercell, the closest distance between two MoS<sub>2</sub> nanoribbons is larger than 12 Å.

The optimized lattice constants of hexagonal graphene and MoS<sub>2</sub> monolayer are 2.47 and 3.20 Å, respectively. Thus, 3DGM-5Z supercell contains 48 C atoms, 15 Mo atoms and 30 S atoms with a small lattice mismatch of 2.4%, as illustrated in Figure 1 (a). The unit cell of 3DGM-5A structure contains 132 C atoms, 25 Mo atoms and 50 S atoms with a 1.9% lattice mismatch, as showed in Figure 1 (b).

In order to know the relative stability of the 3DGMs, the formation energy is used to evaluate the interactions between graphene and MoS<sub>2</sub> nanoribbon. The formation energy of 3DGM contains two parts: the first part is to cut the monolayer MoS<sub>2</sub> into nanoribbon, and the second one is to combine the MoS<sub>2</sub> nanoribbon with graphene. In the following, the formation energy for each part is considered. The formation energies of the part 1, the part 2 and the whole process are referred as  $E_{f1}$ ,  $E_{f2}$  and  $E_f$ , respectively, which are defined as

$$E_{f1} = (E_{\text{ribbon}} - E_{\text{monolayer}}) / N_{\text{edge}} \quad (1)$$

$$E_{f2} = (E_{\text{3DGM}} - E_{\text{ribbon}} - E_{\text{graphene}}) / N_{\text{edge}} \quad (2)$$

$$E_f = E_{f1} + E_{f2} \quad (3)$$

Where  $E_{\text{3DGM}}$ ,  $E_{\text{ribbon}}$ ,  $E_{\text{monolayer}}$  and  $E_{\text{graphene}}$  are the energies of the considered 3DGM structure, MoS<sub>2</sub> nanoribbon building blocks, monolayer MoS<sub>2</sub> with the same number of atoms and graphene building blocks, respectively.  $N_{\text{edge}}$  indicates the numbers of edge units in the zigzag or armchair MoS<sub>2</sub> nanoribbon building blocks. The calculated  $E_{f1}$ ,  $E_{f2}$  and  $E_f$  of different 3DGMs are listed in Table 1.

It should be noted that  $E_{f1}$  of zigzag MoS<sub>2</sub> nanoribbons are lower than those of the armchair MoS<sub>2</sub>. It indicates the zigzag

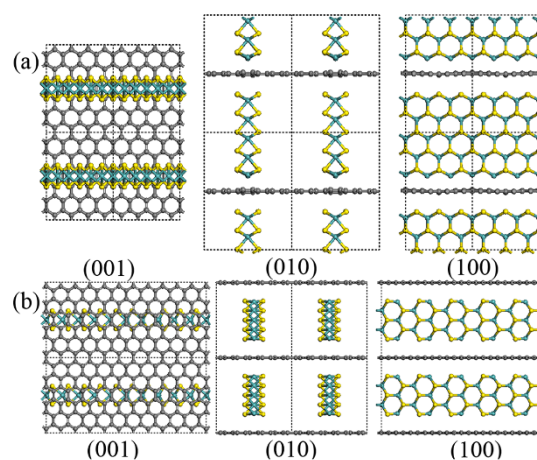


**Figure 1 | Top and side views of the (a) zigzag type 3DGM-5Z and (b) armchair type 3DGM-5A along the different directions, respectively.** Here, 3DGM-5Z presents the system contains 5 atom-layer zigzag MoS<sub>2</sub> and graphene. The grey, yellow, and blue balls represent carbon atoms, sulfur atoms, and molybdenum atoms, respectively.

MoS<sub>2</sub> nanoribbons are more stable than armchair ones, which agrees well with previous theoretical and experimental studies<sup>31,32</sup>. All the  $E_{f2}$  of 3DGM are negative, indicating the relative interaction between graphene and MoS<sub>2</sub> nanoribbon. Interestingly, the  $E_f$  of all 3DGM-*n*Z structures is smaller than that of 3DGM-*n*A. 3DGM-5Z exhibits the lowest formation energy of  $-0.204$  eV, as listed in bold in Table 1. The small or even negative formation energy implies that zigzag MoS<sub>2</sub> nanoribbon is easier to form the 3DGM hybrid structure with graphene. Therefore, the 3DGM-5Z as an example structure is used to further study the electronic properties.

To further explore the thermodynamic stability of the 3DGM hybrid structures, FPMD calculations were carried out at the temperature of  $T = 500$  K with a time step of 0.5 fs. The results show that structures of all considered 3DGM have no obvious change after 1000 fs FPMD simulations. The honeycomb structure of graphene and MoS<sub>2</sub> nanoribbon does not change at  $T = 500$  K, but the nearest-neighbor distances between Mo and C atoms are slightly increased. As shown in Figure 2, the average bond length of Mo-C in 3DGM-5Z increases from the initial 2.33 Å to 2.44 Å at  $T = 500$  K due to the thermal vibration of atoms. These results imply that all the considered 3DGM structures should be thermodynamically stable at room temperature. More importantly, 3DGM can avoid the aggregation between the layered structures, thus such 3D structure should be more stable than the single layer one.

**The electronic structures of the 3DGM.** It is well-known that graphene is zero-gap material, while zigzag and armchair MoS<sub>2</sub>

**Table 1 | Formation energies of different 3DGM structures.** Both zigzag and armchair MoS<sub>2</sub> are considered, along with their different thickness. 3DGM-*n*Z (3DGM-*n*A) represents a 3DGM structure that contains *n* atom-layer thickness zigzag (armchair) MoS<sub>2</sub> nanoribbon. The most stable 3DGM is labeled in bold

Structures	$E_{f1}$ (eV)	$E_{f2}$ (eV)	$E_f$ (eV)
3DGM-2Z	1.106	-0.748	0.358
3DGM-3Z	1.038	-0.870	0.168
3DGM-4Z	0.798	-0.786	0.012
<b>3DGM-5Z</b>	<b>0.667</b>	<b>-0.871</b>	<b>-0.204</b>
3DGM-3A	1.305	-0.505	0.800
3DGM-4A	1.271	-0.580	0.691
3DGM-5A	1.168	-0.526	0.642

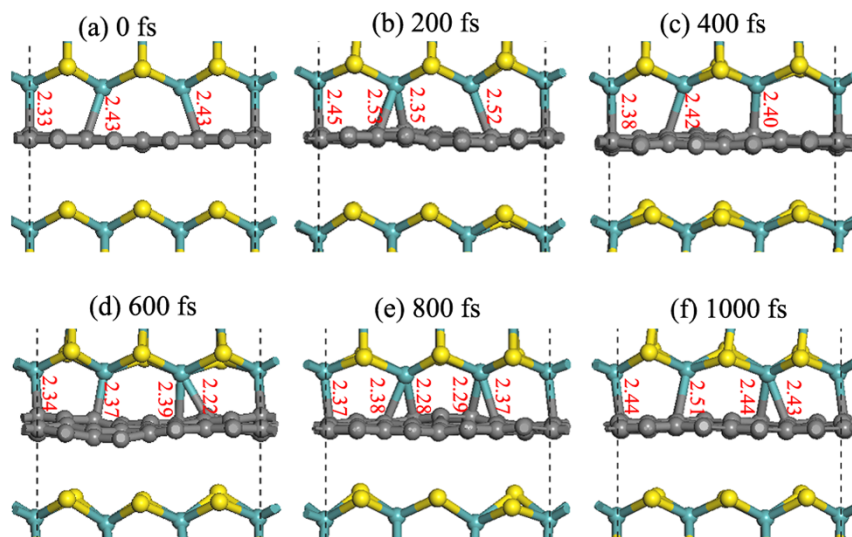


**Figure 2 |** The interface structure evolution and Mo-C bond vibration of the 3DGM-5Z as a function of the FPMD simulation time. Here, 3DGM-5Z presents the system contains 5 atom-layer zigzag MoS<sub>2</sub> and graphene. The unit of bond length is Å. The grey, yellow, and glaucous balls represent carbon atoms, sulfur atoms, and molybdenum atoms, respectively.

nanoribbons are metal and semiconductor, respectively<sup>31</sup>. Thus it is instructive to know the electronic structures of the 3DGM hybrid structures with different thickness and edges in MoS<sub>2</sub> nanoribbons. The band structures and partial charge distributions of the representative 3DGM-4Z and 3DGM-5Z are presented in Figures 3 (a) and (b), respectively. The calculated band structures suggest that 3DGM-4Z is metal, but 3DGM-5Z is semiconductor with a very small band gap of 0.01 eV. In order to check the accuracy of our results on the electronic properties, both the hybrid HSE06 functional<sup>33,34</sup> and spin-orbit coupling effects<sup>35</sup> are employed to examine the electronic properties of 3DGM. The calculated electronic structures with hybrid HSE06 functional or spin-orbit coupling show that the 3DGM-4Z structures remain metal properties. The band gap of 3DGM-5Z is 0.01 eV with PBE, and band gap of 3DGM-5Z increases to 0.15 eV with hybrid HSE06 functional. Besides spin-orbit coupling calculations also show a relative large bandgap of 0.08 eV for 3DGM-5Z. Thus the PBE functional calculations exhibit reasonable electronic properties of 3DGM.

Band decomposed charge density indicates that the band structures near the Fermi level are closely related to the configurations of the joint zone between graphene and MoS<sub>2</sub>. The metal features of 3DGM-4Z are mainly contributed by the atoms at the joint zone. For the semiconductive 3DGM-5Z, the charge density of valence band maximum (VBM) and conduction band minimum (CBM) is located on the S atoms at the joint zone. As shown in the previous work<sup>31,36</sup>, the MoS<sub>2</sub> nanoribbons generally exhibits magnetism, the spin polarization of zigzag MoS<sub>2</sub> nanoribbon were considered in our calculations. Different from MoS<sub>2</sub> nanoribbons, 3DGM exhibits a very small total magnetic moment. For example, the total magnetic moment of 3DGM-5Z is about 0.001μ<sub>B</sub> in the supercell.

The similar odd-even effect of band structures also exists in the 3DGM structures containing armchair MoS<sub>2</sub> nanoribbons. As depicted in Figures 3 (c) and (d), the band structures of 3DGM-*n*A change from metal to semiconductor (with a band gap of 0.25 eV) as *n* increases from 4 to 5. The electrons near the Fermi level in 3DGM-4A is mainly distributed on the Mo atoms, as shown in Figure 3(c). The VBM and CBM states of the 3DGM-5A localize on the different zone of the armchair MoS<sub>2</sub> nanoribbons, due to the small lattice mismatch<sup>37</sup> of the graphene and MoS<sub>2</sub> edge type.

To explore the electronic properties of 3DGM, the electron localization function (ELF) and charge density difference ( $\Delta\rho$ ) of the

3DGM are investigated. The ELF is a position-dependent function with  $0 < \text{ELF} < 1$ ; and the value of  $\text{ELF} = 0.5$  corresponds to the electron-gas like pair probability<sup>38</sup>. The ELF of 3DGM-5Z and 3DGM-5A are showed in Figures 4 (a) and (c), respectively. The result shows that ELF is very small between graphene and the MoS<sub>2</sub> nanoribbon in both 3DGM-5Z and 3DGM-5A, demonstrating the absence of any directional covalent-type bonds.

To further understand the bonding of graphene and MoS<sub>2</sub> nanoribbon, we studied the charge density difference of the 3DGM-5Z and 3DGM-5A, as indicated in Figures 4 (b) and (d), respectively. The charge density difference is defined as<sup>39</sup>

$$\Delta\rho = \rho_{3\text{DGM}}(r) - \rho_{\text{ribbon}}(r) - \rho_{\text{graphene}}(r) \quad (4)$$

Where  $\rho_{3\text{DGM}}(r)$ ,  $\rho_{\text{ribbon}}(r)$ , and  $\rho_{\text{graphene}}(r)$  are the charge densities of the relaxed 3DGM, MoS<sub>2</sub> nanoribbons, and clean graphene surfaces, respectively. In the 3DGM-5Z, the obvious charge redistribution in the joint zone suggests the ionic bonding between Mo and C atoms. Few of the charge transfer from C to S atoms which indicate the weak bonding between edge S and C atoms. To understand the physical origin of charge transfer between the graphene and zigzag MoS<sub>2</sub> nanoribbons, the work function of graphene sheet and zigzag MoS<sub>2</sub> nanoribbon are examined relative to the vacuum level. The calculated work function of graphene sheet is 4.17 eV. The work function of Mo atom edge and S atom edge of zigzag MoS<sub>2</sub> nanoribbons are 4.95 and 5.02 eV, respectively. Thus the electron of graphene can transfer to zigzag MoS<sub>2</sub> nanoribbons when they form the 3D structures. It is also noted that no charge transfer between the graphene nanosheets and armchair MoS<sub>2</sub> nanoribbons in the 3DGM-5A. There is just a small charge redistribution in the edge Mo atoms. Thus, two edges of armchair MoS<sub>2</sub> nanoribbons combine with the graphene by the weak vdW interactions. The relatively weak bonding of graphene and armchair MoS<sub>2</sub> nanoribbons also can be deduced by the formation energy calculations (see  $E_{f2}$  in Table 1).

**Adsorption and diffusion of Li on the 3DGM-5Z.** The recent studies suggest that MoS<sub>2</sub> nanostructures are more attractive for lithium-ion battery applications since the Li diffusion path in nanostructures could be significantly shortened<sup>40</sup>. For example, the Li diffusion energy barrier in MoS<sub>2</sub> monolayer (0.21 eV) is much lower than that in MoS<sub>2</sub> bulk (0.49 eV). More interestingly, its adsorption energy in the zigzag MoS<sub>2</sub> nanoribbons increases by a value of 2.73–3.62 eV due to edge effects<sup>40</sup>. The 3DGM has large

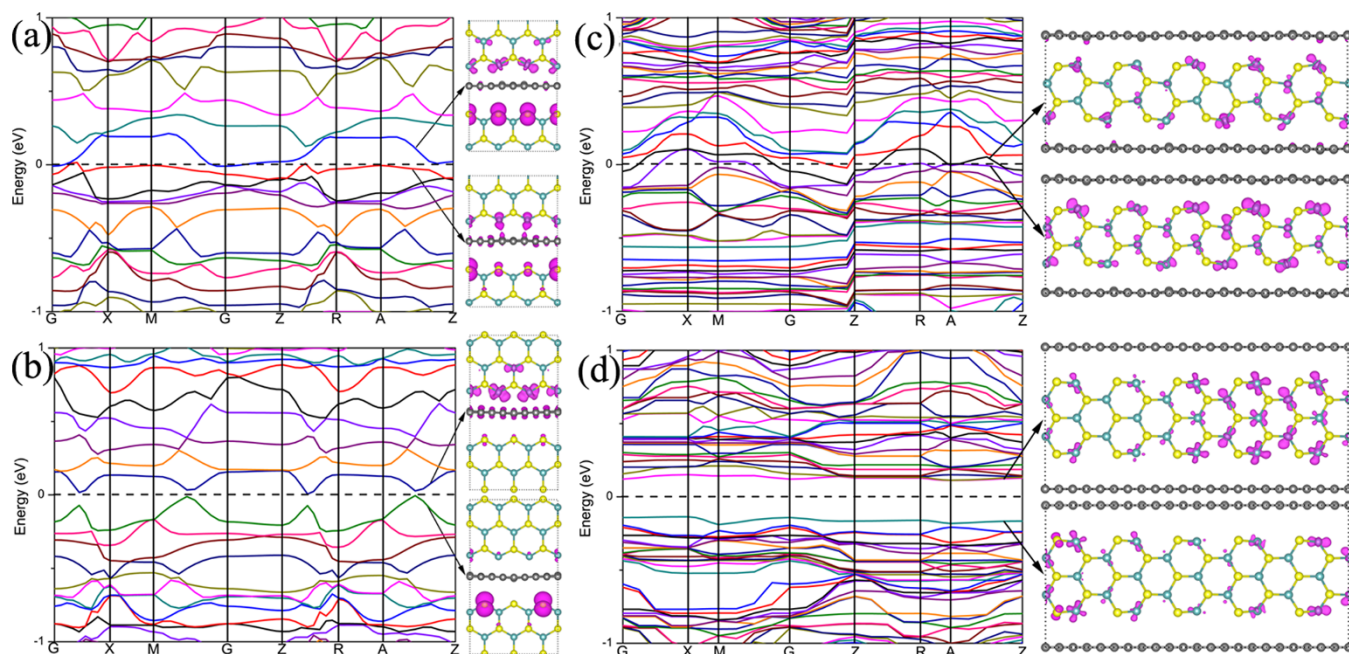


**Figure 3** | The band structures and band decomposed charge densities of the (a) 3DGM-4Z, (b) 3DGM-5Z, (c) 3DGM-4A and (d) 3DGM-5A. 3DGM-nZ (3DGM-nA) represents a 3DGM structure that contains n atom-layer thickness zigzag (armchair) MoS<sub>2</sub> nanoribbon. The corresponding highest occupied molecule state (HOMO) and lowest unoccupied molecule state (LUMO) are shown on upper and low panel in violet color as well. The grey, yellow, and glaucous balls represent carbon atoms, sulfur atoms, and molybdenum atoms, respectively.

surface area and more Li adsorption sites. Recent experiments also demonstrate that 3DGM hybrid structures exhibits highly reversible capacity and excellent cycling performance<sup>26,27</sup> in Li batteries. Previous theory calculations have shown that the largest adsorption energies of Li on graphene is 1.096 eV<sup>41</sup>, which is much lower than that on zigzag MoS<sub>2</sub> nanoribbon. Thus, Li atom prefers to adsorb on the zigzag MoS<sub>2</sub> nanoribbon rather than on graphene in the 3DGM structures. It should be noted that a high Li adsorption energy<sup>42</sup> or high Li intercalation voltage is crucial to ensure the thermodynamic stability in the cathodes for lithium ion batteries. 2D MoS<sub>2</sub> nanosheets are not ideal candidates for cathode materials because that they exhibit the relatively low Li adsorption energies of about 2.12 eV. MoS<sub>2</sub> nanoribbons can increase the Li adsorption energy (3.62 eV) due to the edge effect<sup>40</sup>. However, the bare zigzag MoS<sub>2</sub> nanoribbon only has a very limited number of edge atoms.

In order to know whether the three dimensional 3DGM can improve the adsorption of Li on MoS<sub>2</sub>, the Li adsorption on 3DGM-5Z is firstly explored. For the adsorption of Li on 3DGM, there are many possible sites because of the interface. For example, as for the top site of Mo atoms, there are 10 different sites for the top site of Mo atoms (labeled as T1–T10) and eight hollow sites for Mo-S six-membered ring (labeled as H1–H8), and the four interfacial side sites (Labeled as S1–S4). All non-equivalent Li adsorption positions of the 3DGM-5Z are marked in the Figure 5 (a), and the corresponding Li adsorption energies are listed in the Table 2. The adsorption energy of Li on the top sites decreases stepwise from the S-C interface to the Mo-C interface. The similar regulation also exists in the Li adsorption on the hollow and side sites of zigzag MoS<sub>2</sub> nanoribbon. The adsorption energies of Li on the S atom edges are significantly enhanced due to the interface effect of the graphene and zigzag

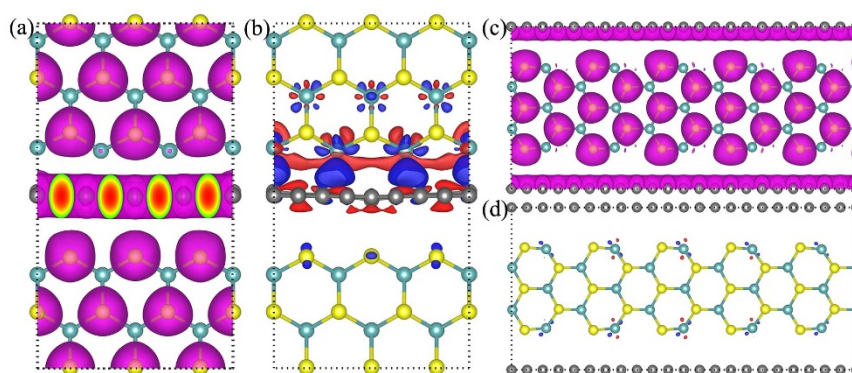


**Figure 4** | The electron localization function (ELF) of (a) 3DGM-5Z and (c) 3DGM-5A. Violet isosurfaces correspond to the ELF (the isovalue is 0.5). The corresponding charge density difference of 3DGM-5Z and 3DGM-5A are shown in (b) and (d), respectively. Blue and red isosurfaces correspond to the accumulation and depletion of electronic densities (the isovalue is 0.02 e/Å<sup>3</sup>). 3DGM-nZ (3DGM-nA) represents a 3DGM structure that contains n atom-layer thickness zigzag (armchair) MoS<sub>2</sub> nanoribbon. The grey, yellow, and glaucous balls represent carbon atoms, sulfur atoms, and molybdenum atoms, respectively.



MoS<sub>2</sub> nanoribbon. Similar phenomena were also found in bare zigzag graphene nanoribbons, which are believed to be responsible for the enhanced Li adsorption strength at the edge sites<sup>40</sup>. Here, the three dimensional 3DGM hybrid structure, assembling zigzag MoS<sub>2</sub> nanoribbons with graphene nanosheets, can effectively improve the Li adsorption on MoS<sub>2</sub> with an even larger Li adsorption energy of 3.82 eV, compared with either MoS<sub>2</sub> nanoribbons.

To examine the edge effect on the Li mobility, the diffusion of Li along the S-C interface of 3DGM-5Z is examined. Since the adsorption energies of Li on S-C interfaces are obviously larger than those on the inner sites or the interfaces, the Li atom should migrate along the S-C interface. The diffusion route is thus along the periodic direction of zigzag MoS<sub>2</sub> nanoribbon: T1 → H1 → T2 → H2 → T2' → H1' → T1, as highlighted by blue dotted lines in Figure 5 (a), and the calculated diffusion barriers are shown in Figure 5 (b). It can be seen that a Li atom only needs to conquer an energy barrier of 0.30 eV to migrate from a T1 site to another, passing through the H1, T2 and H2 site. To compare the diffusion barriers, the Li diffusion path is divided to three sections by the nearest top sites, marked as T1 → H1 → T2, T2 → H2 → T2' and T2' → H1' → T1, and the diffusion barriers are 0.26, 0.24 and 0.26 eV, respectively. The Li diffusion barrier of the nearest top sites is within 0.26 eV. In order to check the effect of zero-point energy term on the reaction barrier, the typical diffusion process from T2-H2 was checked. The result shows that the zero-point energy term reduces the reaction barrier by 0.02 eV, and the reaction barrier becomes 0.24 eV including the zero-point energy term. Thus, Li diffusion barrier on the 3DGM-5Z is slightly larger than that on the MoS<sub>2</sub> monolayer (0.21 eV), but is much lower than that on that of bulk MoS<sub>2</sub> (0.49 eV)<sup>40</sup>. Larger adsorption energy and smaller diffusion barrier of Li atoms on 3DGM-5Z make it an ideal material for the cathode of lithium ion batteries.

## Discussion

We performed systematic first-principle calculations for the studies of the atomic configuration, thermodynamics stability and electronic properties of various 3D Graphene/MoS<sub>2</sub> hybrid structure. The calculated formation energies reveal that the 3DGM are easily assembled by graphene nanosheet and MoS<sub>2</sub> nanoribbons. The first principles molecular dynamics simulations confirmed that the 3DGM structures should be thermodynamically stable. The electronic structures of 3DGM are greatly affected by the thickness

**Table 2** | The calculated adsorption energies ( $E_{\text{adsorb}}$ ) of Li atom on 3DGM-5Z structure for all possible absorption positions (The corresponding sites are shown in Figure 5). The most stable adsorption energies are shown in bold

Position	$E_{\text{adsorb}}$ (eV)	Position (eV)	$E_{\text{adsorb}}$ (eV)	Position	$E_{\text{adsorb}}$ (eV)
<b>T1</b>	<b>3.82</b>	<b>H1</b>	<b>3.61</b>	<b>S1</b>	<b>3.12</b>
T2	3.76	H2	3.55	S2	3.30
T3	3.30	H3	3.08	S3	0.34
T4	3.28	H4	3.06	S4	0.34
T5	3.09	H5	2.91		
T6	3.08	H6	2.91		
T7	2.95	H7	2.75		
T8	3.01	H8	2.82		
T9	2.76				
T10	2.79				

and edge type of MoS<sub>2</sub> nanoribbons. The 3DGM with odd-layer thickness MoS<sub>2</sub> nanoribbon is semiconductor, while the one with even-layer thickness MoS<sub>2</sub> nanoribbon exhibits metallic feature. The 3DGM structures not only own the large surface area and high stability to avoid the aggregation, but also they exhibit the large adsorption energy and small diffusion energy barrier for Li storage. Thus such three dimensional hybrid materials have great potential as high-performance cathode materials for lithium ion battery.

## Methods

In this work, two DFT packages have been used. The first-principles structure and energy calculations are mainly performed using the Vienna Ab Initio Simulation Package (VASP)<sup>43,44</sup>. Projector augmented-wave (PAW) pseudopotentials<sup>45</sup> were used to account electron-ion interactions. The generalized gradient approximation (GGA) with the PBE function<sup>46</sup> was used to treat the exchange-correlation interaction between electrons. The energy cutoff was set to 500 eV and  $3 \times 3 \times 3$  Monkhorst-Pack scheme was used to sample Brillouin zone. The full geometry optimizations are carried out with the convergence thresholds of  $10^{-6}$  eV and  $5 \times 10^{-3}$  eV/Å for total energy and ionic force, respectively. DFT-D2<sup>47</sup> approach was used to describe the vdW interactions between layers.

The mixed Gaussian and plane-wave basis set code CP2K/Quickstep package<sup>48</sup> has been used for the first principles molecular dynamics (FPMD) and Li diffusion barrier calculations. The wave functions of the valence electrons are expanded in terms of Gaussian functions with molecularly optimized double-zeta polarized basis sets (m-DZVP)<sup>49</sup>. For the auxiliary basis set of plane waves a 320 Ry cut-off is used. In the FPMD simulations the canonical ensemble was employed<sup>50,51</sup> with a target

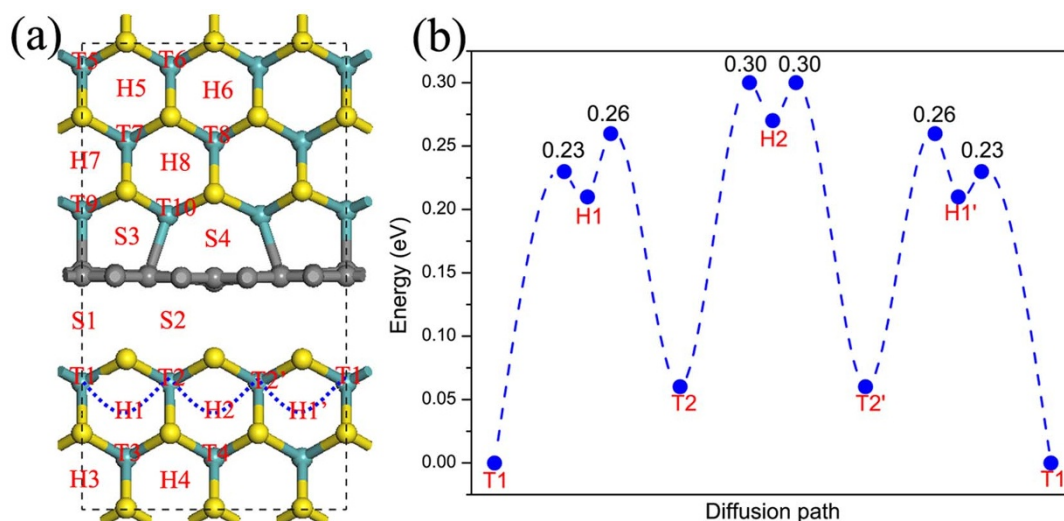


**Figure 5** | (a) All the possible Li atom adsorption sites on 3DGM-5Z marked by the red characters and the most possible diffusion path denoted by blue dotted lines. (b) The diffusion barrier of Li atom on 3DGM-5Z along the diffusion path (T1 → H1 → T2 → H2 → T2' → H1' → T1). The grey, yellow, and glaucous balls represent carbon atoms, sulfur atoms, and molybdenum atoms, respectively.



temperature of 300 K, maintained with a Nosé-Hoover chain thermostat. Calculations of diffusion barrier of Li were performed using the climbing-image nudged-elastic-band method (CI-NEB)<sup>52</sup> with nine points along the reaction paths.

- Novoselov, K. S. Electric Field Effect in Atomically Thin Carbon Films. *Science* **306**, 666–669, doi:10.1126/science.1102896 (2004).
- Neto, A. H. C., Peres, N. M. R., Novoselov, K. S. & Geim, A. K. The electronic properties of graphene. *Rev. Mod. Phys.* **81**, 109–162, doi:10.1103/RevModPhys.81.109 (2009).
- Du, A., Zhu, Z. & Smith, S. C. Multifunctional Porous Graphene for Nanoelectronics and Hydrogen Storage: New Properties Revealed by First Principle Calculations. *J. Am. Chem. Soc.* **132**, 2876–2877, doi:10.1021/ja100156d (2010).
- Li, Y., Zhang, R.-Q., Lin, Z. & Van Hove, M. A. Energetics and dynamics of a new type of extended line defects in graphene. *Nanoscale* **4**, 2580–2583, doi:10.1039/C2NR30185G (2012).
- Li, Y., Zhou, Z., Shen, P. & Chen, Z. Spin Gapless Semiconductor–Metal–Half-Metal Properties in Nitrogen-Doped Zigzag Graphene Nanoribbons. *ACS Nano* **3**, 1952–1958, doi:10.1021/nn9003428 (2009).
- Quhe, R. *et al.* Tunable band gap in few-layer graphene by surface adsorption. *Sci. Rep.* **3**, doi:10.1038/srep01794 (2013).
- Wangmo, S. *et al.* Strong interactions and charge transfers between a charged benzene molecule and multilayer graphenes. *J. Mater. Chem.* **22**, 23380–23386, doi:10.1039/C2JM35634A (2012).
- Du, A. *et al.* Hybrid Graphene/Titania Nanocomposite: Interface Charge Transfer, Hole Doping, and Sensitization for Visible Light Response. *J. Phys. Chem. Lett.* **2**, 894–899, doi:10.1021/jz2002698 (2011).
- Li, D., Muller, M. B., Gilje, S., Kaner, R. B. & Wallace, G. G. Processable aqueous dispersions of graphene nanosheets. *Nat. Nano* **3**, 101–105, doi:10.1038/nnano.2007.451 (2008).
- Cao, X., Yin, Z. & Zhang, H. Three-dimensional graphene materials: preparation, structures and application in supercapacitors. *Energy Environ. Sci.* **7**, 1850, doi:10.1039/c4ee00050a (2014).
- Cao, X. *et al.* Preparation of novel 3D graphene networks for supercapacitor applications. *Small* **7**, 3163–3168, doi:10.1002/smll.201100990 (2011).
- Dong, X. *et al.* 3D Graphene Foam as a Monolithic and Macroporous Carbon Electrode for Electrochemical Sensing. *ACS Appl. Mater. Inter.* **4**, 3129–3133, doi:10.1021/am300459m (2012).
- Yin, S., Niu, Z. & Chen, X. Assembly of graphene sheets into 3D macroscopic structures. *Small* **8**, 2458–2463, doi:10.1002/smll.201102614 (2012).
- Wang, X. *et al.* Three-dimensional strutted graphene grown by substrate-free sugar blowing for high-power-density supercapacitors. *Nat. Commun.* **4**, 2905, doi:10.1038/ncomms3905 (2013).
- Choi, B. G., Yang, M., Hong, W. H., Choi, J. W. & Huh, Y. S. 3D macroporous graphene frameworks for supercapacitors with high energy and power densities. *ACS Nano* **6**, 4020–4028 (2012).
- Dong, X. *et al.* 3D Graphene-Cobalt Oxide Electrode for High-Performance Supercapacitor and Enzymeless Glucose Detection. *ACS Nano* **6**, 3206–3213 (2012).
- Huang, Y. *et al.* Assembly of Tin Oxide/Graphene Nanosheets into 3D Hierarchical Frameworks for High-Performance Lithium Storage. *Chem. Sus. Chem.* **6**, 1510–1515, doi:10.1002/cssc.201300109 (2013).
- Mak, K. F., Lee, C., Hone, J., Shan, J. & Heinz, T. F. Atomically Thin MoS<sub>2</sub>: A New Direct-Gap Semiconductor. *Phys. Rev. Lett.* **105**, 136805 (2010).
- Chianelli, R. R. *et al.* Catalytic Properties of Single Layers of Transition Metal Sulfide Catalytic Materials. *Catal. Rev.* **48**, 1–41, doi:10.1080/01614940500439776 (2006).
- Xie, J. *et al.* Controllable Disorder Engineering in Oxygen-incorporated MoS<sub>2</sub> Ultrathin Nanosheets for Efficient Hydrogen Evolution. *J. Am. Chem. Soc.* **135**, 17881 (2013).
- Lukowski, M. A. *et al.* Enhanced hydrogen evolution catalysis from chemically exfoliated metallic MoS<sub>2</sub> nanosheets. *J. Am. Chem. Soc.* **135**, 10274–10277, doi:10.1021/ja404523s (2013).
- Du, G. *et al.* Superior stability and high capacity of restacked molybdenum disulfide as anode material for lithium ion batteries. *Chem. Commun.* **46**, 1106–1108, doi:10.1039/B920277C (2010).
- Huang, X., Zeng, Z. & Zhang, H. Metal dichalcogenide nanosheets: preparation, properties and applications. *Chem. Soc. Rev.* **42**, 1934–1946, doi:10.1039/c2cs35387c (2013).
- Xiao, J. *et al.* Exfoliated MoS<sub>2</sub> Nanocomposite as an Anode Material for Lithium Ion Batteries. *Chem. Mater.* **22**, 4522–4524, doi:10.1021/cm101254j (2010).
- Yang, G., Wang, Y. & Ma, Y. A Stable, Magnetic, and Metallic Li<sub>3</sub>O<sub>4</sub> Compound as a Discharge Product in a Li–Air Battery. *J. Phys. Chem. Lett.* **5**, 2516–2521, doi:10.1021/jz501160z (2014).
- Cao, X. *et al.* Preparation of MoS<sub>2</sub>-Coated Three-Dimensional Graphene Networks for High-Performance Anode Material in Lithium-Ion Batteries. *Small* **9**, 3433–3438, doi:10.1002/smll.201202697 (2013).
- Yu, H. *et al.* Three-Dimensional Hierarchical Architectures Constructed by Graphene/MoS<sub>2</sub> Nanoflake Arrays and Their Rapid Charging/Discharging Properties as Lithium-Ion Battery Anodes. *Chem. – Euro. J.* **19**, 5818–5823, doi:10.1002/chem.201300072 (2013).
- Jiang, X., Zhao, J., Li, Y.-L. & Ahuja, R. Tunable Assembly of sp<sup>3</sup>Cross-Linked 3D Graphene Monoliths: A First-Principles Prediction. *Adv. Funct. Mater.* **23**, 5846–5853, doi:10.1002/adfm.201301077 (2013).
- Zhang, S., Wang, Q., Kawazoe, Y. & Jena, P. Three-dimensional metallic boron nitride. *J. Am. Chem. Soc.* **135**, 18216–18221, doi:10.1021/ja410088y (2013).
- Tang, Z.-K., Zhang, H., Liu, H., Lau, W.-M. & Liu, L.-M. A novel three dimensional semimetallic MoS<sub>2</sub>. *J. Appl. Phys.* **115**, 204302, doi:10.1063/1.4879241 (2014).
- Li, Y., Zhou, Z., Zhang, S. & Chen, Z. MoS<sub>2</sub> Nanoribbons: High Stability and Unusual Electronic and Magnetic Properties. *J. Am. Chem. Soc.* **130**, 16739–16744, doi:10.1021/ja805545x (2008).
- Wang, Z. *et al.* Mixed Low-Dimensional Nanomaterial: 2D Ultranarrow MoS<sub>2</sub> Inorganic Nanoribbons Encapsulated in Quasi-1D Carbon Nanotubes. *J. Am. Chem. Soc.* **132**, 13840–13847, doi:10.1021/ja1058026 (2010).
- Heyd, J., Scuseria, G. E. & Ernzerhof, M. Hybrid functionals based on a screened Coulomb potential. *J. Chem. Phys.* **118**, 8207–8215, doi:10.1063/1.1564060 (2003).
- Heyd, J., Scuseria, G. E. & Ernzerhof, M. Erratum: “Hybrid functionals based on a screened Coulomb potential” [J. Chem. Phys. 118, 8207 (2003)]. *J. Chem. Phys.* **124**, 219906, doi:10.1063/1.2204597 (2006).
- Dresselhaus, G. Spin-Orbit Coupling Effects in Zinc Blende Structures. *Physical Review* **100**, 580–586, doi:10.1103/PhysRev.100.580 (1955).
- Kou, L. *et al.* Tuning Magnetism and Electronic Phase Transitions by Strain and Electric Field in Zigzag MoS<sub>2</sub> Nanoribbons. *The Journal of Physical Chemistry Letters* **3**, 2934–2941, doi:10.1021/jz301339e (2012).
- Kang, J., Li, J., Li, S. S., Xia, J. B. & Wang, L. W. Electronic structural Moire pattern effects on MoS<sub>2</sub>/MoSe<sub>2</sub> 2D heterostructures. *Nano Lett.* **13**, 5485–5490, doi:10.1021/nl4030648 (2013).
- Herbst, J. & Hector, L. Energetics of the Li amide/Li imide hydrogen storage reaction. *Phys. Rev. B* **72**, 125120, doi:10.1103/PhysRevB.72.125120 (2005).
- Preuss, M., Schmidt, W. & Bechstedt, F. Coulombic Amino Group-Metal Bonding: Adsorption of Adenine on Cu(110). *Phys. Rev. Lett.* **94**, 236102, doi:10.1103/PhysRevLett.94.236102 (2005).
- Li, Y., Wu, D., Zhou, Z., Cabrera, C. R. & Chen, Z. Enhanced Li Adsorption and Diffusion on MoS<sub>2</sub> Zigzag Nanoribbons by Edge Effects: A Computational Study. *J. Phys. Chem. Lett.* **3**, 2221–2227, doi:10.1021/jz300792n (2012).
- Chan, K. T., Neaton, J. B. & Cohen, M. L. First-principles study of metal adatom adsorption on graphene. *Phys. Rev. B* **77**, 235430, doi:10.1103/PhysRevB.77.235430 (2008).
- Sun, C. & Searles, D. J. Lithium Storage on Graphdiyne Predicted by DFT Calculations. *J. Phys. Chem. C* **116**, 26222–26226, doi:10.1021/jp309638z (2012).
- Kresse, G. & Furthmüller, J. Efficient iterative schemes for ab initio total energy calculations using a plane-wave basis set. *Phys. Rev. B* **54**, 11169–11186 (1996).
- Kresse, G. & Furthmüller, J. Efficiency of ab-initio total energy calculations for metals and semiconductors using a plane-wave basis set. *Comput. Mater. Sci.* **6**, 15–50, doi:DOI: 10.1016/0927-0256(96)00008-0 (1996).
- Kresse, G. & Joubert, D. From ultrasoft pseudopotentials to the projector augmented-wave method. *Phys. Rev. B* **59**, 1758–1775 (1999).
- Perdew, J. P., Burke, K. & Ernzerhof, M. Generalized Gradient Approximation Made Simple. *Phys. Rev. Lett.* **77**, 3865–3868 (1996).
- Wu, X., Vargas, M. C., Nayak, S., Lotrich, V. & Scoles, G. Towards extending the applicability of density functional theory to weakly bound systems. *J. Chem. Phys.* **115**, 8748–8757, doi:10.1063/1.1412004 (2001).
- VandeVondele, J. *et al.* Quickstep: Fast and accurate density functional calculations using a mixed Gaussian and plane waves approach. *Comput. Phys. Commun.* **167**, 103–128, doi:10.1016/j.cpc.2004.12.014 (2005).
- VandeVondele, J. & Hutter, J. Gaussian basis sets for accurate calculations on molecular systems in gas and condensed phases. *The Journal of chemical physics* **127**, 114105, doi:10.1063/1.2770708 (2007).
- Liu, L.-M., Li, S.-C., Cheng, H., Diebold, U. & Selloni, A. Growth and Organization of an Organic Molecular Monolayer on TiO<sub>2</sub>: Catechol on Anatase (011). *J. Am. Chem. Soc.* **133**, 7816–7823, doi:10.1021/ja200001r (2011).
- Liu, L.-M. *et al.* Enhanced Thermal Decomposition of Nitromethane on Functionalized Graphene Sheets: Ab Initio Molecular Dynamics Simulations. *J. Am. Chem. Soc.* **134**, 19011–19016, doi:10.1021/ja3058277 (2012).
- Henkelman, G., Uberuaga, B. P. & Jónsson, H. A climbing image nudged elastic band method for finding saddle points and minimum energy paths. *J. Chem. Phys.* **113**, 9901–9904, doi:10.1063/1.1329672 (2000).

## Acknowledgments

This work was supported by the National Natural Science Foundation of China (No. 51222212), the CAEP foundation (Grant No. 2012B0302052), the Hunan Provincial Natural Science Foundation of China No. 2015JJ6013), the Science Foundation of Hengyang Normal University (No. 13B41), the MOST of China (973 Project, Grant NO. 2011CB922200), the Hunan Provincial Applied Basic Research Base of Optoelectronic Information Technology (No. GDXX002), and the Construct Program for Key Disciplines in Hunan Province.

## Author contributions

The idea was conceived by L.L. The simulation was performed by Z.T. The data analyses were performed by Z.T., D.Z., W.L. and L.L. This manuscript was written by Z.T., Y.Z. and L.L. All authors discussed the results and contributed to the paper.



## Additional information

**Competing financial interests:** The authors declare no competing financial interests.

**How to cite this article:** Tang, Z.-K., Zhang, Y.-N., Zhang, D.-Y., Lau, W.-M. & Liu, L.-M. The stability and electronic properties of novel three-dimensional graphene-MoS<sub>2</sub> hybrid structure. *Sci. Rep.* 4, 7007; DOI:10.1038/srep07007 (2014).



This work is licensed under a Creative Commons Attribution-NonCommercial-NoDerivs 4.0 International License. The images or other third party material in this article are included in the article's Creative Commons license, unless indicated otherwise in the credit line; if the material is not included under the Creative Commons license, users will need to obtain permission from the license holder in order to reproduce the material. To view a copy of this license, visit <http://creativecommons.org/licenses/by-nc-nd/4.0/>